Bi-allelic Mutations in *FAM149B1* Cause Abnormal Primary Cilium and a Range of Ciliopathy Phenotypes in Humans

Ranad Shaheen,[1] Nan Jiang,[2] Fatema Alzahrani,[1] Nour Ewida,[1] Tarfa Al-Sheddi,[1] Eman Alobeid,[1] Damir Musaev,[2] Valentina Stanley,[2] Mais Hashem,[1] Niema Ibrahim,[1] Firdous Abdulwahab,[1] Abduljabbar Alshenqiti,[4] Fatma Mujgan Sonmez,[3] Nadia Saqati,[4] Hamad Alzaidan,[4] Mohammad M. Al-Qattan,[5] Futwan Al-Mohanna,[6] Joseph G. Gleeson,[2] and Fowzan S. Alkuraya[1,7,8,*]

Ciliopathies are clinical disorders of the primary cilium with widely recognized phenotypic and genetic heterogeneity. In two Arab consanguineous families, we mapped a ciliopathy phenotype that most closely matches Joubert syndrome (hypotonia, developmental delay, typical facies, oculomotor apraxia, polydactyly, and subtle posterior fossa abnormalities) to a single locus in which a founder homozygous truncating variant in *FAM149B1* was identified by exome sequencing. We subsequently identified a third Arab consanguineous multiplex family in which the phenotype of Joubert syndrome/oral-facial-digital syndrome (OFD VI) was found to co-segregate with the same founder variant in *FAM149B1*. Independently, autozygosity mapping and exome sequencing in a consanguineous Turkish family with Joubert syndrome highlighted a different homozygous truncating variant in the same gene. *FAM149B1* encodes a protein of unknown function. Mutant fibroblasts were found to have normal ciliogenesis potential. However, distinct cilia-related abnormalities were observed in these cells: abnormal accumulation IFT complex at the distal tips of the cilia, which assumed bulbous appearance, increased length of the primary cilium, and dysregulated SHH signaling. We conclude that FAM149B1 is required for normal ciliary biology and that its deficiency results in a range of ciliopathy phenotypes in humans along the spectrum of Joubert syndrome.

In most non-dividing eukaryotic cells, the centrioles assume the role of a basal body from which the formation of an elongated microtubule-based structure is initiated, eventually forming the cilium with its modified membrane.[1] Motile cilia perform a multitude of functions ranging from locomotion in adult sperm cells to controlling the flow of the nodal fluid very early in embryonic development, and their defects are known as primary ciliary dyskinesia syndromes.[2] The closely related primary cilium lacks the microtubule arrangement required for motility yet it mediates an expansive list of physiological and developmental functions by acting as a signaling hub and a mechanical sensor.[3,4] Abnormalities of the primary cilium are known clinically as ciliopathy syndromes.

Ciliopathies are highly variable in their clinical presentation, and the range of phenotypic severity extends from early embryonic lethality to adult-onset isolated eye or kidney disease.[5–7] Joubert syndrome and related disorders (JSRD) are classical ciliopathies that are characterized by typical cerebellar malformations with an associated ocular movement disorder. Developmental delay with hypotonia and intellectual disability are typical features, and many children have characteristic facies.[8] Similar to other ciliopathies, JSRD can be variable even within sibships, e.g., the posterior fossa involvement may be absent in some siblings but present in others.[5] In addition, clinical presentation of JSRD may significantly overlap with another ciliopathy known as oral-facial-digital syndrome (OFD) and the resulting hybrid phenotype is often referred to as OFD VI (MIM: 277170).[9]

Remarkable progress has been achieved in recent years in deciphering the molecular basis of JSRD, and many of the 34 genes listed in OMIM in connection with this phenotype have been identified only in the last decade thanks to the advent of next-generation genome sequencing. This has resulted in an impressive yield in the diagnostic workup of JSRD-affected case subjects with a recent large study suggesting that only 7% remain unexplained after exome sequencing.[5] This suggests that the residual genetic heterogeneity likely involves genes with increasingly small contribution to the overall mutation spectrum, which necessitates international collaboration as suggested previously.[10] Here, we describe *FAM149B1* as one such gene and suggest its involvement in ciliary homeostasis.

The index case subject in family 1 (17DG0722) is the first born child to first cousin parents and presented with developmental delay, hypotonia, oculomotor apraxia, ptosis, and mesoaxial polydactyly (Table 1 and Figure 1A). Although brain MRI did not reveal the typical "molar tooth sign," the clinical diagnosis of JSRD was made, and he was enrolled in an IRB-approved research protocol (KFSHRC

[1]Department of Genetics, King Faisal Specialist Hospital and Research Center, PO Box 3354, Riyadh 11211, Saudi Arabia; [2]Laboratory for Pediatric Brain Disease, Howard Hughes Medical Institute, Department of Neurosciences, University of California, San Diego, La Jolla, CA 92093, USA; [3]Karadeniz Technical University, Faculty of Medicine, Department of Child Neurology, Retired Lecturer, Trabzon 61080, Turkey; [4]Department of Medical Genetics, King Faisal Specialist Hospital and Research Center, Riyadh 1211, Saudi Arabia; [5]Department of Surgery, King Saudi University, Riyadh 11451, Saudi Arabia; [6]Department of Cell Biology, King Faisal Specialist Hospital and Research Center, PO Box 245, Riyadh 11211, Saudi Arabia; [7]Saudi Human Genome Program, King Abdulaziz City for Science and Technology, Riyadh 12371, Saudi Arabia; [8]Department of Anatomy and Cell Biology, College of Medicine, Alfaisal University, Riyadh 11533, Saudi Arabia
*Correspondence: falkuraya@kfshrc.edu.sa
https://doi.org/10.1016/j.ajhg.2019.02.018.

Table 1. Summary of Clinical and Mutations Data for the Study Cohort

Case ID	17DG0722 (Family 1_V:1)	12DG2038 (Family 2_V:1)	12DG0596 (Family 3_II:4)	MTI-2230 (Family 4_IV:3)
Variant	c.356_357delAG (p.Lys119Ilefs*18)	c.356_357delAG (p.Lys119Ilefs*18)	c.356_357delAG (p.Lys119Ilefs*18)	c.439C>T (p.Gln147*)
Age (Year)	2	17	3	4
Gender	M	M	M	M
Ethnicity	Arab	Arab	Arab	Turkish
Consanguinity	y	y	y	y
DD/ID	y	y	y	y
OMA/strabismus	y	y	y	y
Ptosis	y	y	y	y
Polydactyly	y	y	y	y
MTS on MRI	n	very mild	N/A	y
Others	Joubert facies (prominent forehead, high and rounded eyebrows, upturned nose, anteverted nares, open mouth)	NSHL, normal ERG	macrocephaly (enlarged lateral ventricles on CT), grossly narrow chest with severe pectus carinatum, lusterless hair, normal echocardiography, midline cleft	macrocephaly, lusterless hair, epilepsy, CHD

Abbreviations: CHD, congenital heart disease; CT, computed tomography; DD, developmental delay; ERG, electroretinogram; ID, intellectual disability; MTS, molar tooth sign; NSHL, neurosensory hearing loss.

RAC# 2070023, 2080006, and 2121053) with informed consent after his clinical exome sequencing failed to identify the likely etiology. Autozygome analysis was performed as described before.[11] Exome sequencing was performed on the index subject, and the exome variants were filtered by the coordinates of the candidate autozygome as described before.[12] Additionally, only homozygous coding/splicing variants that are novel/very rare (MAF < 0.001) according to gnomAD and a database of 2,379 ethnically matched exomes were considered. Only one variant remained after applying such filters: *FAM149B1*, GenBank: NM_173348.1; c.356_357del (p.Lys119Ilefs*18) (Figure 2). Despite the complete absence of this variant in the above-mentioned exome cohorts, it was encountered twice in a homozygous state in our cohort of individuals with ciliopathy phenotypes. Case subject 12DG2038, from family 2, is also the first child to a consanguineous couple and presented with developmental delay, oculomotor apraxia, ptosis, and mesoaxial polydactyly and was labeled as JSRD (Table 1 and Figure 1). The other case subject (12DG0596) from family 3, whose parents are distantly related, was referred by a hand surgeon because of suspected OFD VI, which is a hybrid phenotype between oral-facial-digital syndrome and Joubert syndrome. This was based on the typical Y-shaped metacarpal, lusterless hair, and midline cleft lip (OFD features), in addition to ocular movement abnormality, ptosis, and developmental delay (Joubert syndrome features) (Figures 1A and 1E–1G and Table 1). His affected sister has identical clinical features including bilateral hand meso-axial polydactyly with the typical Y-shaped central metacarpal (a specific feature of Varadi syndrome), lusterless hair, and midline cleft lip (OFD features) and ocular movement abnormality, ptosis, and developmental delay (Joubert syndrome features). In addition, she also has high arched palate and clinodactyly of the right 4th and 5th fingers (OFD features), mild sensorineural deafness and mild hypotonia (Joubert features), and mild pectus excavatum. Haplotype analysis confirmed the founder nature of the variant, which resides in a shared homozygous region of 2,030,228 base pairs on chromosome 10:73710638–75740865 (hg19) (Figure 2A). The frameshift deletion variant in exon 4 of *FAM149B1* predicts a frameshift of the protein (GenBank: NP_775483.1) starting from position 119 and the introduction of a premature stop codon leading to the loss of 464 aa of the protein including 90% of DUF3719 domain (the predicted functional domain of FAM149B1 protein). With the help of GeneMatcher,[13] we were able to identify a fourth consanguineous family of Turkish descent with typical Joubert syndrome (Figure 1 and Table 1). Whole-exome sequencing was performed on the index subject (MTI-2230-IV-3) and variants filtered as described above, identifying an apparently truncating (nonsense) homozygous variant in *FAM149B1* (GenBank: NM_173348.1; c.439C>T [p.Gln147*]), which was confirmed by Sanger sequencing to segregate according to a recessive mode of inheritance (Figure 2). The second variant is also predicted to create stop codon at aa 147 leading to the loss of 435 aa of FAM149B1 protein. The Saudi variant and the Turkish variant have a frequency of 0 and 6.637e−6 in gnomAD, respectively, and were absent in ethnically matched exomes (Saudi Human Genome Program collection and Gleeson's lab collection of more than 5,000 exomes).

FAM149B1 encodes a protein of unknown function (family with sequence similarity 149, member B). Available expression data show a strong expression in the early

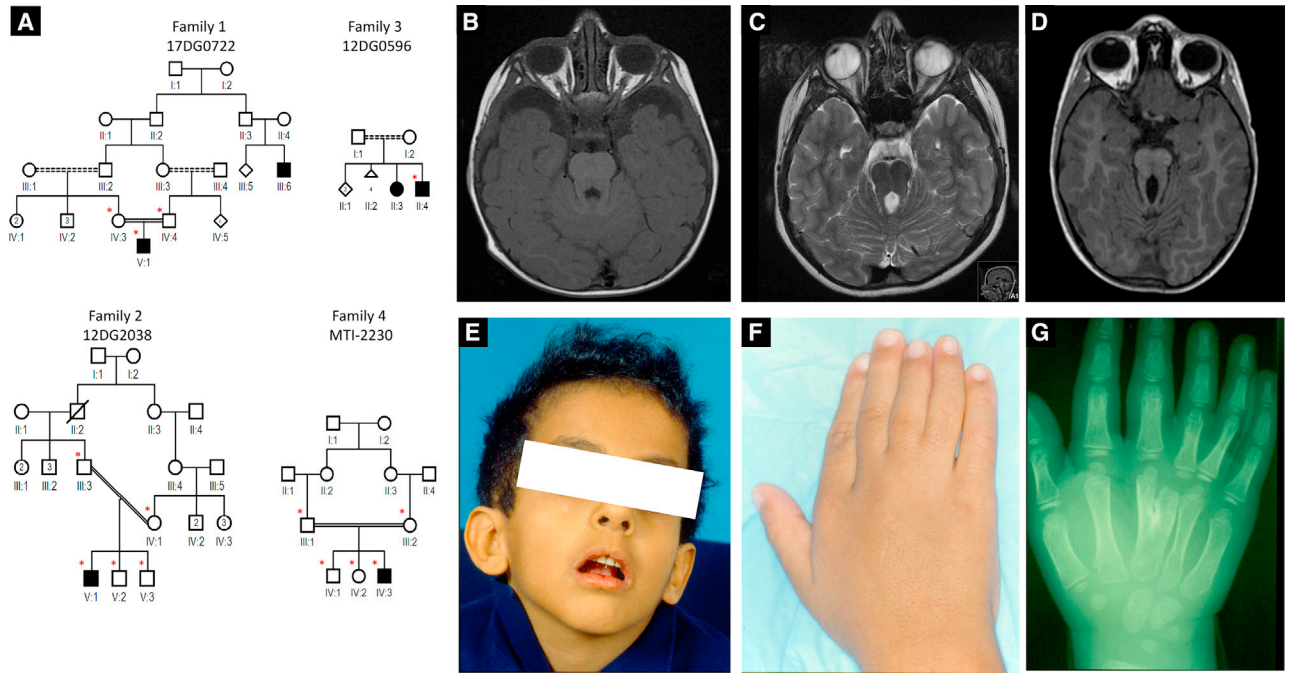

Figure 1. Identification of Four Families with Autosomal-Recessive JSRD
(A) Pedigrees of the four families included in this study showing the consanguineous relationship between parents (asterisks denote individuals whose DNA was available for analysis).
(B–D) Representative MRI images for the affected individuals 17DG0722, 12DG2038, and MTI-2230 showing a range from nearly absent to classical MTS.
(E and F) Facial and hand photos of the affected individual 12DG0596 showing midline notch in the upper lip (Forme Fruste cleft lip; classic of OFD syndrome) and mesoaxial polydactyly.
(G) Hand X-ray of the affected individual 12DG0596 showing the typical Y-shaped metacarpal of OFD VI.

mouse embryonic stages (E8, 9, and 10) in the neuroepithelium followed by the maxillary arches (see Expression Atlas in Web Resources). In order to gain insight into the potential effect of FAM149B1 deficiency on the primary cilium, we obtained a skin biopsy followed by propagation of a primary dermal fibroblast cell line from individual

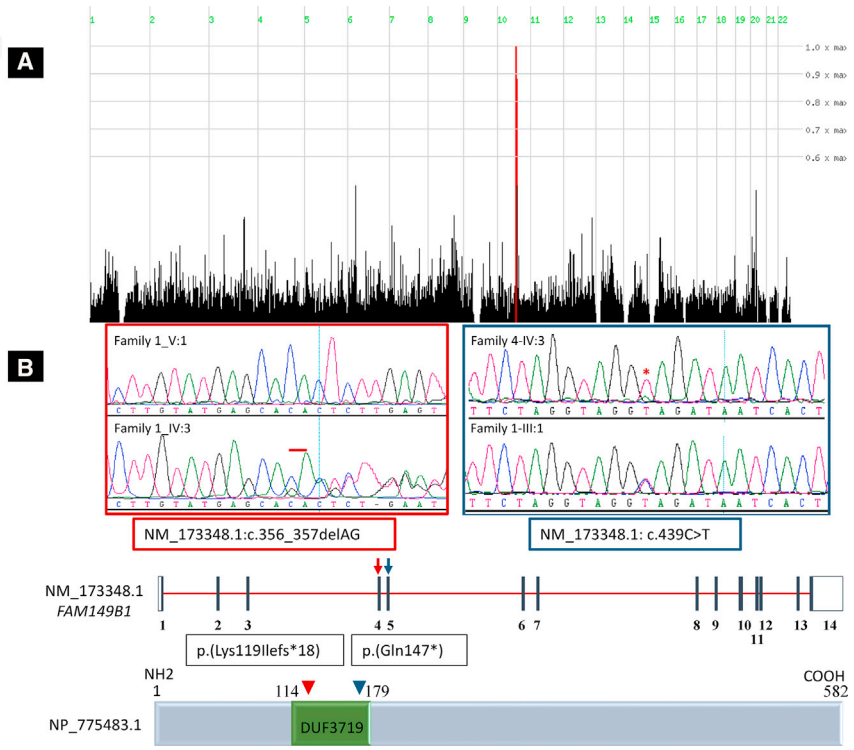

Figure 2. Identification of Two Likely Deleterious Homozygous Variants in *FAM149B1*
(A) HomozygosityMapper image showing a single locus on chromosome 10.
(B) Genomic DNA sequence chromatogram of *FAM149B1* showing the two apparently truncating variants, and a schematic of *FAM149B1* gene (top) and encoded protein (bottom) with the location of the two variants indicated. DUF3719 resemble domain that belongs to DUF families which is annotated as domain with unknown function, found in eukaryotes, approximately 70 amino acids in length with conserved HLR sequence motif and two completely conserved residues (W and H) that may be functionally important.

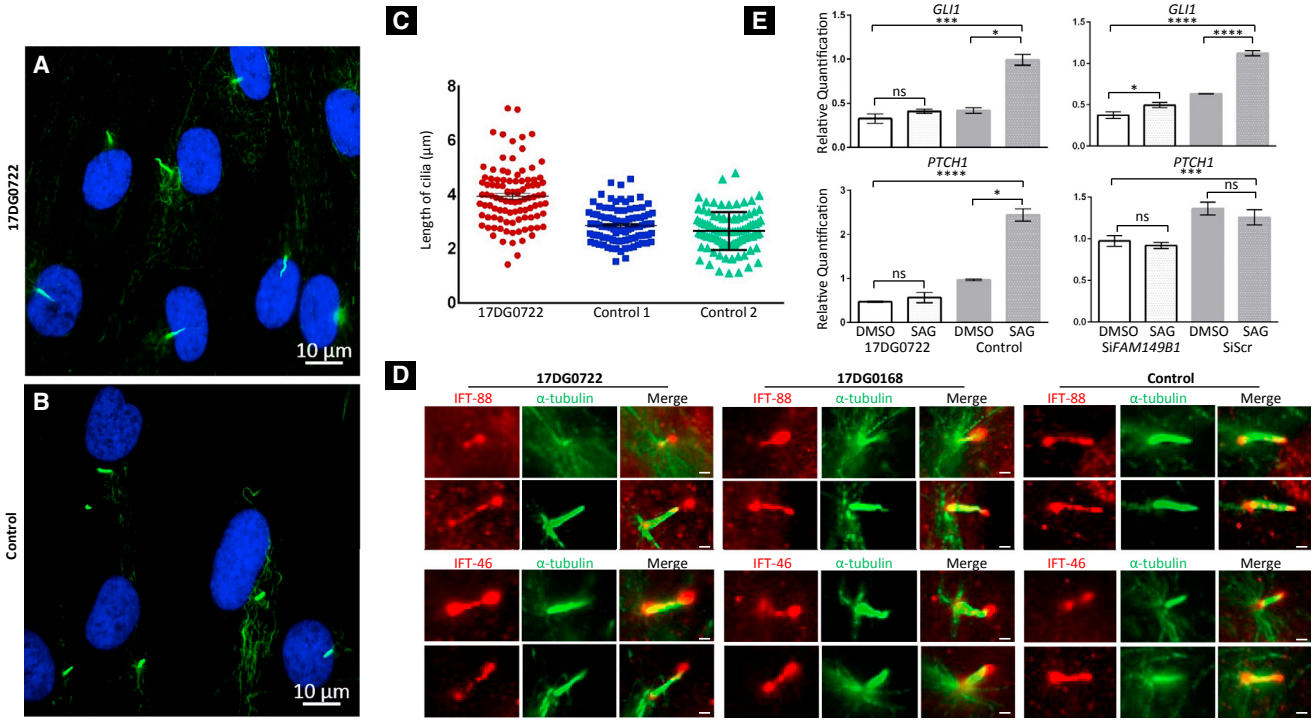

Figure 3. ***FAM149B1*-Related Ciliopathy Is Associated with Impaired Cilia Structure and Function**
(A and B) Immunofluorescence images of the serum-starved fibroblasts from the affected individual in family 1 (A) and control fibroblasts (B) stained for the ciliary marker acetylated α-tubulin (Sigma-Aldrich, T7451) (green) and DNA (blue) showing marked increase in the length of the cilia with normal cilia frequency in the affected individual cells compared to controls. Scale bars represent 10 μm.
(C) Point chart of the ciliary length measured using ImageJ showing significantly longer cilia in the affected individual compared to two control subjects. Bars represent the mean with the SEM, p value < 0.0001.
(D) Immunofluorescence staining images of the affected individual 17DG0722 fibroblast cilia, affected individual 17DG0168 with mutation in *TBC1D32*, and control stained with the ciliary marker acetylated α-tubulin (Sigma-Aldrich, T7451) (green) and IFT-88 (ProteinTech, 13967-1-AP) (red) (top) or IFT-46 (Abcam ab122422) (red) (bottom) showing marked "pooling" of IFT-88 and IFT-46 at the tip with apparent bulging and bulbous morphology. Scale bars represent 1 μm.
(E) Left column: bar graph showing the relative quantification to the mRNA expression of *GLI1* and *PTCH1* which were markedly lower in fibroblasts from the affected individual cells 17DG0722 in family 1 than control fibroblasts in response to Smoothened Agonist (SAG) stimulation of 100 nM for 18 h on the basis of two independent experiments (each performed in triplicate). Right column: bar graph showing the relative quantifications to the mRNA expression of *GLI1* and *PTCH1;* the significantly lower expression of *GLI1* and *PTCH1* and lower induction of *GLI1* in response to SAG stimulation in siRNA of *FAM149B1* transcript in HEK293 cells in comparison to negative control scrambled siRNA. Quantification was based on three independent samples, each run in triplicate. Error bars represent the SEM, statistical significance represents results from two-tailed Student's t test and two-way ANOVA are indicated by *$p < 0.05$, **$p < 0.01$, ***$p < 0.001$, and ****$p < 0.0001$; ns, non-significant.

17DG0722. We first set out to assess the ciliogenesis potential of mutant versus wild-type cells using the standard serum starvation assay.[14] As shown in Figure 3A, there was no significant difference in the number of ciliated cells. However, we did observe an appreciable difference in the length of the cilia, with mutant cells having significantly longer cilia compared to two control subjects (3.9 (1.4–7.2) versus 2.9 μm (1.5–4.6) and 2.7 (1.1–4.8), p value for two-way ANOVA < 0.0001). Furthermore, there was a greater variability of ciliary length in the mutant compared to control cells (SD of 1.1 versus 0.6 and 0.7, respectively). Ciliary length control is an incompletely understood complex process that involves, among others, intraflagellar transport (IFT)-related mechanisms.[15–17] To investigate this possibility, we evaluated the staining pattern of the IFT-88 and IFT-46 (members of the IFT-B complex involved in the anterograde transport of cargo in the cilium) and IFT-122 (a member of IFT-A complex involved in the retrograde transport). While the typical punctate staining pattern along the entire shaft of the cilium was maintained in the mutant cells for the three IFT proteins tested, we noticed marked "pooling" of IFT-88 and IFT-46 at the tip with apparent bulging (Figures 3D and S1). This bulbous morphology has been observed in several cilia-related mutants and is thought to represent impaired retrograde transport.[18,19]

While the function of FAM149B1 is unknown, we were intrigued by the findings of Huttlin and colleagues who used high-throughput affinity-purification mass spectrometry to identify interacting partners of 2,594 human proteins in HEK293T cells.[20] The resulting database showed experimental evidence of FAM149B1 interaction with TBC1D32 (also called BROMI). This is potentially relevant because in 2014, we published a report on a family with a

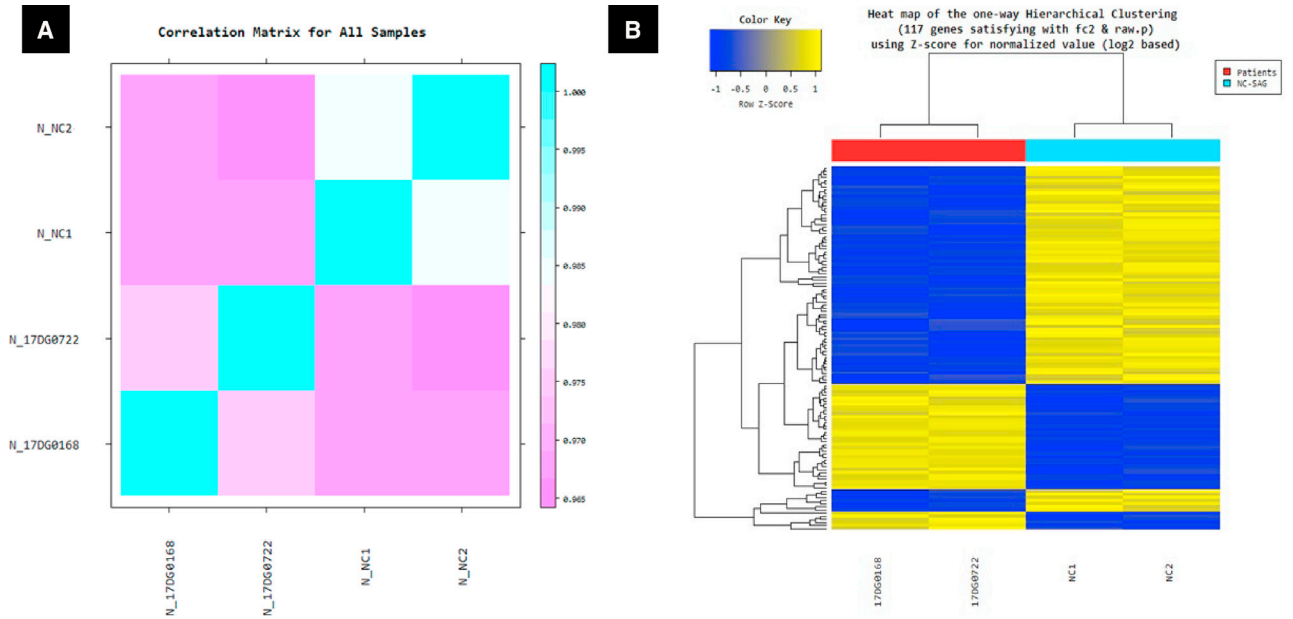

Figure 4. Gene Expression Analysis (RNA Sequencing) of *FAM149B1* Mutant Fibroblast Cells Cluster with *TBC1D32* Mutant Fibroblast Cells

(A) Correlation matrix showing the similarity between samples of 17DG0722 and 17DG0168 fibroblast cells versus two control subjects are obtained through Pearson's coefficient of the Log2(FPKM+1) value. For range: $-1 \leq r \leq 1$, the closer the value is to 1, the more similar the samples are.

(B) Heatmap of one-way hierarchical clustering (distance metric = Euclidean distance, linkage method = complete) analysis of DEG (differentially expressed genes) was performed on affected individual 17DG0722 and 17DG0168 fibroblast cells versus two control subjects using FPKM. The result showed 117 genes differentially expressed which satisfied $|fc| \geq 2$ and independent t test raw p value < 0.05 conditions. Blue denotes normalized downregulation; yellow denotes upregulation (see attached scale above). The detailed DEG data and the list of the 117 genes are in Table S1.

homozygous splice site variant that was confirmed to lead to in-frame deletion of 141 base pair in *TBC1D32*, which we proposed to be causative of the OFD phenotype observed in the index individual.[21] This association is further supported by the report of knockout mice that display typical ciliopathy features.[22] Furthermore, although the neural tube of *bromi* mutants exhibits comparable cilia frequency to control littermates, they exhibit an abnormal swollen or bulbous morphology.[22] In addition, cilia from cells harboring mutant *Ccrk*, encoding the other known protein that physically interacts with BROMI, exhibit the phenotypes of swelling at the distal ends and defect in the regulation of the length.[23]

To further investigate the association between FAM149B1 and TBC1D32, we established fibroblast cells from individual 17DG0168 with the previously published splice site mutation in *TBC1D32*.[21] The *TBC1D32* mutant fibroblasts not only display the same abnormal accumulation of IFT complex at the tip of the cilia (Figure 3D) but also clustered with FAM149B1 mutant fibroblasts upon gene expression analysis using RNA-seq versus two controls (Figure 4). Furthermore, Co-IP experiment confirmed that FAM149B1 and TBC1D32 are indeed interacting partners (Figure 5).

In order to probe the potentially deleterious consequence of the observed ciliary structural abnormalities on the ciliary function, we used the well-established assay of SAG-induced upregulation of the SHH signaling pathway using *GLI1* and *PTCH1* as a readout. Our results demonstrated significant dysregulation of the SHH signaling in the mutant cells compared to controls, and HEK293 cells subjected to *FAM149B1* siRNA knockdown recapitulated that dysregulation (Figures 3E and S2). This supports the notion that FAM149B1 deficiency results in not only impaired ciliary structure but also function with consequent development of a ciliopathy phenotype.

In summary, we demonstrate two independent homozygous truncating alleles in *FAM149B1* in four families with a range of ciliopathy phenotypes mostly consistent with JSRD and the closely related OFD VI. All previously published genes in connection with these phenotypes have been implicated in various aspects of ciliary biology and our functional characterization of FAM149B1 seems consistent with this pattern. We, therefore, propose the establishment of *FAM149B1*-related ciliopathy in humans. Given the presumably truncating nature of the alleles identified in this study and the relatively mild ciliopathy phenotype, it will be of interest to observe the phenotypic manifestations of milder bi-allelic variants and whether they are sufficient to cause the development of a recognizable ciliopathy or perhaps a milder non-specific phenotype. The development of a mouse model should shed more light on the precise role of FAM149B1 during development.

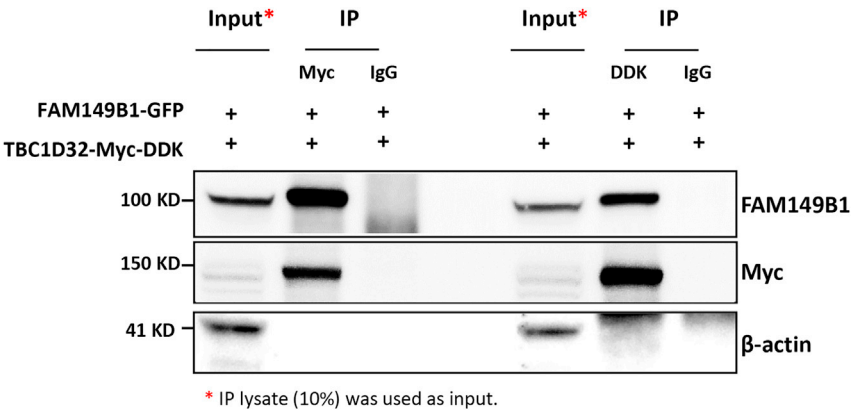

Figure 5. FAM149B1 Interacts with TBC1D32

Co-immunoprecipitation (Co-IP) assay to test the interaction between FAM149B1 and TBC1D32 was performed using protein lysates from HEK293 cells co-transfected with GFP-FAM149B1 and MYC-DDK-TBC1D32 plasmids. TBC1D32 was immunoprecipitated from the transfected HEK293 cells using MYC or DDK antibody and the immunoprecipitated materials were analyzed by SDS-PAGE. After transfer, membranes were probed using antibodies to FAM149B1, MYC and β-actin. Rabbit and mouse immunoglobulin G antibodies were used as negative controls in the immunoprecipitation reaction. IP lysates (10%) was used as inputs.

Supplemental Data

Supplemental Data can be found with this article online at https://doi.org/10.1016/j.ajhg.2019.02.018.

Acknowledgment

We thank the families for their enthusiastic participation. We also thank the genotyping and sequencing core facilities at King Faisal Specialist Hospital and Research Center for their technical help and the Yale Center for Mendelian Disorders (U54HG006504 to R. Lifton, M. Gunel, M. Gerstein, and S. Mane) for sequencing support and analysis. This work was supported by the King Salman Center for Disability Research (F.S.A.), King Abdulaziz City for Science and Technology (13-BIO1113-20, F.S.A.), the Saudi Human Genome Program (F.S.A.), the Howard Hughes Medical Institute, and the National Institute of Neurological Disorders and Stroke (R01NS048453).

Declaration of Interests

The authors declare no competing interests.

Received: March 20, 2018
Accepted: February 14, 2019
Published: March 21, 2019

Web Resources

Ensembl Genome Browser, http://www.ensembl.org/index.html
Expression Atlas, https://www.ebi.ac.uk/gxa/
GenBank, https://www.ncbi.nlm.nih.gov/genbank/
GnomAD, https://gnomad.broadinstitute.org/
HomozygosityMapper, http://www.homozygositymapper.org/
ImageJ, https://imagej.nih.gov/ij/download.html
InterPro, https://www.ebi.ac.uk/interpro/entry/IPR022194
Online Mendelian Inheritance in Man (OMIM), https://www.omim.org/
UCSC Genome Browser, http://genome.ucsc.edu/

References

1. Ishikawa, H., and Marshall, W.F. (2011). Ciliogenesis: building the cell's antenna. Nat. Rev. Mol. Cell Biol. *12*, 222–234.
2. Fliegauf, M., Benzing, T., and Omran, H. (2007). When cilia go bad: cilia defects and ciliopathies. Nat. Rev. Mol. Cell Biol. *8*, 880–893.
3. Fry, A.M., Leaper, M.J., and Bayliss, R. (2014). The primary cilium: guardian of organ development and homeostasis. Organogenesis *10*, 62–68.
4. Goetz, S.C., and Anderson, K.V. (2010). The primary cilium: a signalling centre during vertebrate development. Nat. Rev. Genet. *11*, 331–344.
5. Shaheen, R., Szymanska, K., Basu, B., Patel, N., Ewida, N., Faqeih, E., Al Hashem, A., Derar, N., Alsharif, H., Aldahmesh, M.A., et al.; Ciliopathy WorkingGroup (2016). Characterizing the morbid genome of ciliopathies. Genome Biol. *17*, 242.
6. Shamseldin, H.E., Kurdi, W., Almusafri, F., Alnemer, M., Alkaff, A., Babay, Z., Alhashem, A., Tulbah, M., Alsahan, N., Khan, R., et al. (2018). Molecular autopsy in maternal–fetal medicine. Genet. Med. *20*, 420–427.
7. Patel, N., Aldahmesh, M.A., Alkuraya, H., Anazi, S., Alsharif, H., Khan, A.O., Sunker, A., Al-Mohsen, S., Abboud, E.B., Nowilaty, S.R., et al. (2016). Expanding the clinical, allelic, and locus heterogeneity of retinal dystrophies. Genet. Med. *18*, 554–562.
8. Alazami, A.M., Alshammari, M.J., Salih, M.A., Alzahrani, F., Hijazi, H., Seidahmed, M.Z., Abu Safieh, L., Aldosary, M., Khan, A.O., and Alkuraya, F.S. (2012). Molecular characterization of Joubert syndrome in Saudi Arabia. Hum. Mutat. *33*, 1423–1428.
9. Al-Qattan, M.M., Shaheen, R., and Alkuraya, F.S. (2017). Expanding the allelic disorders linked to TCTN1 to include Varadi syndrome (Orofaciodigital syndrome type VI). Am. J. Med. Genet. A. *173*, 2439–2441.
10. Boycott, K.M., Rath, A., Chong, J.X., Hartley, T., Alkuraya, F.S., Baynam, G., Brookes, A.J., Brudno, M., Carracedo, A., den Dunnen, J.T., et al. (2017). International cooperation to enable the diagnosis of all rare genetic diseases. Am. J. Hum. Genet. *100*, 695–705.
11. Alkuraya, F.S. (2010). Autozygome decoded. Genet. Med. *12*, 765–771.
12. Alkuraya, F.S. (2013). The application of next-generation sequencing in the autozygosity mapping of human recessive diseases. Hum. Genet. *132*, 1197–1211.
13. Sobreira, N., Schiettecatte, F., Valle, D., and Hamosh, A. (2015). GeneMatcher: a matching tool for connecting investigators with an interest in the same gene. Hum. Mutat. *36*, 928–930.

14. Shaheen, R., Faqeih, E., Shamseldin, H.E., Noche, R.R., Sunker, A., Alshammari, M.J., Al-Sheddi, T., Adly, N., Al-Dosari, M.S., Megason, S.G., et al. (2012). POC1A truncation mutation causes a ciliopathy in humans characterized by primordial dwarfism. Am. J. Hum. Genet. *91*, 330–336.
15. Silverman, M.A., and Leroux, M.R. (2009). Intraflagellar transport and the generation of dynamic, structurally and functionally diverse cilia. Trends Cell Biol. *19*, 306–316.
16. Rosenbaum, J.L., and Witman, G.B. (2002). Intraflagellar transport. Nat. Rev. Mol. Cell Biol. *3*, 813–825.
17. Keeling, J., Tsiokas, L., and Maskey, D. (2016). Cellular mechanisms of ciliary length control. Cells *5*, 6.
18. Shah, A.S., Farmen, S.L., Moninger, T.O., Businga, T.R., Andrews, M.P., Bugge, K., Searby, C.C., Nishimura, D., Brogden, K.A., Kline, J.N., et al. (2008). Loss of Bardet-Biedl syndrome proteins alters the morphology and function of motile cilia in airway epithelia. Proc. Natl. Acad. Sci. USA *105*, 3380–3385.
19. Tsao, C.-C., and Gorovsky, M.A. (2008). Tetrahymena IFT122A is not essential for cilia assembly but plays a role in returning IFT proteins from the ciliary tip to the cell body. J. Cell Sci. *121*, 428–436.
20. Huttlin, E.L., Ting, L., Bruckner, R.J., Gebreab, F., Gygi, M.P., Szpyt, J., Tam, S., Zarraga, G., Colby, G., Baltier, K., et al. (2015). The BioPlex network: a systematic exploration of the human interactome. Cell *162*, 425–440.
21. Adly, N., Alhashem, A., Ammari, A., and Alkuraya, F.S. (2014). Ciliary genes TBC1D32/C6orf170 and SCLT1 are mutated in patients with OFD type IX. Hum. Mutat. *35*, 36–40.
22. Ko, H.W., Norman, R.X., Tran, J., Fuller, K.P., Fukuda, M., and Eggenschwiler, J.T. (2010). Broad-minded links cell cycle-related kinase to cilia assembly and hedgehog signal transduction. Dev. Cell *18*, 237–247.
23. Snouffer, A., Brown, D., Lee, H., Walsh, J., Lupu, F., Norman, R., Lechtreck, K., Ko, H.W., and Eggenschwiler, J. (2017). Cell Cycle-Related Kinase (CCRK) regulates ciliogenesis and Hedgehog signaling in mice. PLoS Genet. *13*, e1006912.

The American Journal of Human Genetics, Volume *104*

Supplemental Data

Bi-allelic Mutations in *FAM149B1* Cause Abnormal Primary Cilium and a Range of Ciliopathy Phenotypes in Humans

Ranad Shaheen, Nan Jiang, Fatema Alzahrani, Nour Ewida, Tarfa Al-Sheddi, Eman Alobeid, Damir Musaev, Valentina Stanley, Mais Hashem, Niema Ibrahim, Firdous Abdulwahab, Abduljabbar Alshenqiti, Fatma Mujgan Sonmez, Nadia Saqati, Hamad Alzaidan, Mohammad M. Al-Qattan, Futwan Al-Mohanna, Joseph G. Gleeson, and Fowzan S. Alkuraya

Supplement Materials and Methods

Transcriptome Expression Profiling

Skin fibroblasts cells of the affected individuals 17DG0722 and 17DG0168 and of age-matched control individuals (n = 2) were processed for transcriptome sequencing. The cells were treated with SAG (Smoothened Agonist) in Opti-MEM-reduced serum medium at a concentration of 100 nM for 16 h and the total RNA were extracted using the QIAamp RNA Mini Kit (Qiagen Inc., Germantown, MD) protocol. RNA and the NGS library quality (size and quantity) control (QC) were checked using Agilent Technologies 2100 Bioanalyzer using a DNA 1000 chip, Illumina qPCR Quantification Protocol Guide and Roche's Rapid library standard Quantification. TruSeq Stranded mRNA LT Sample Prep Kit was used and the library was prepared using TruSeq Stranded mRNA Sample Preparation Guide, Part # 15031047 Rev. E followed by sequencing using NovaSeq 6000 System. The reads were mapped to reference genome with HISAT2, splice-aware aligner and Transcript is assembled by StringTie with aligned reads. The FPKM (Fragments Per Kilobase of transcript per Million Mapped reads) value or the RPKM (Reads Per Kilobase of transcript per Million mapped reads) is used as a normalization value and the Expression profiles are represented as read count and normalization value which is based on transcript length and depth of coverage. Functional annotation and gene-set enrichment analysis were performed using GO and KEGG database on differentially expressed genes with known annotation.

Relative quantification RT-PCR

Total RNA from cell were extracted using the QIAamp RNA Mini Kit (Qiagen Inc., Germantown, MD) and DNase treated by the RNase-Free DNase Set (Qiagen), according to the manufacturer's recommendations. Preparation of the cDNA was carried out using the iScript™ cDNA synthesis kit and poly-T oligonucleotide primers (Applied Biosystems, Carlsbad, CA). The primer sequences for the desired genes are listed in the table *below.* The relative quantification (q) RT-PCR for the expression was performed using SYBR green and Applied Biosystems 7500 Fast Real-Time PCR System.

	Forward	Reverse
GLI1	AGAGAGACCAACAGCTGC	TCATCTGGGCTGGGAATC
PTCH1	ACGATGGAGTCCTTGCCTAC	TTCTCAGCCTTGTTTCAGG
SUFU	ACCCGCTCCAGGTTACC	GTGCCAGGACACATGGTC
HHIP	GGAGCCTTATTTGGACATTCAC	TCATCCCATCACCAAGAATG
SMO	GCAGGTGGATGGGGACTC	CATTGGCCTGACATAGCACA
GAPDH	GGTGAAGGTCGGAGTCAAC	ATGGGTGGAATCATATTGGA
FAM149B1	GACACAAGTTCCCAAAGCAAGT	GCCTACCTAGAATCCTGAGGTG

Figure S1

A) Immunofluorescent staining images of the affected individual 17DG0722 fibroblast cilia and control stained with the ciliary marker acetylated α-tubulin (Sigma-Aldrich, T7451) (green) and IFT-122 (Santa Cruz Biotechnology, sc-102612) (red) showing similar pattern of IFT-122 staining in the affected individual cilia as compared with control cilia. B) Confocal staining images of the affected individual 17DG0722 fibroblast cilia and control stained with the centrosome marker gamma tubulin (Sigma-Aldrich, T6557) (green) and retrograde marker IFT-88 (ProteinTech, 13967-1-AP) (red). Scale bars represent 1 μm

Figure S2

A) Bar Graph showing the relative quantification to the mRNA expression of *HHIP,* and *SMO and SUFU* which were markedly lower in fibroblasts from the affected individual cells 17DG0722 in family 1 than control fibroblasts. B) Bar graph showing the efficiency of *FAM149B1* siRNA in HEK293 cells compared to negative control scrambled siRNA (siScr) as quantified by qRT-PCR for the *FAM149B1* transcript. C) Bar Graph showing the relative quantification to the mRNA expression of *HHIP,* and *SMO and SUFU* which were significantly lower in *FAM149B1* siRNA in HEK293 cells than to negative control scrambled siRNA. Error bars represent the SEM, statistical significance represents results from two-tailed Student's t-test and two-way ANOVA are indicated by * $p < 0.05$, ** $p < 0.01$, *** $p < 0.001$ and **** $p < 0.0001$. ns (non-significant).

Figure S1: *FAM149B1*-related ciliopathy is associated with impaired ciliary structure

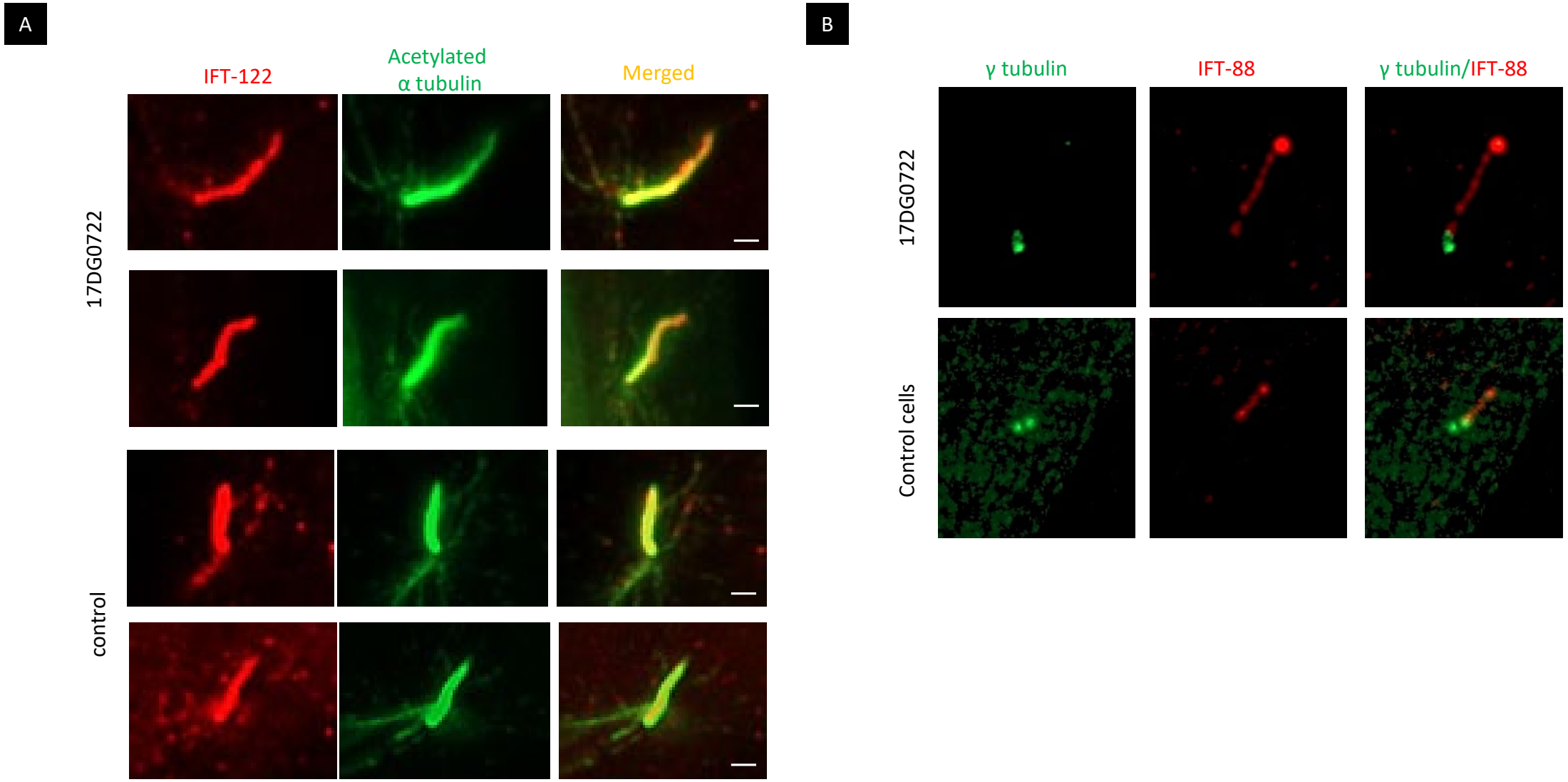

Figure S2: *FAM149B1*-related ciliopathy is associated with impaired ciliary function